JGR Oceans

RESEARCH ARTICLE
10.1029/2023JC020369

Special Section:
Physical processes, sediment transport and morphodynamics of estuaries and coastal seas

Estuarine Exchange Flow in the Salish Sea

Parker MacCready[1] and W. Rockwell Geyer[2]

[1]School of Oceanography, University of Washington, Seattle, WA, USA, [2]Woods Hole Oceanographic Institution, Woods Hole, MA, USA

Key Points:

- The volume transport of the estuarine exchange flow in the Salish Sea increases with stronger tidal transport
- However, the landward salt transport due to the estuarine exchange flow decreases with stronger tidal transport

Correspondence to:
P. MacCready,
pmacc@uw.edu

Citation:
MacCready, P., & Geyer, W. R. (2024). Estuarine exchange flow in the Salish Sea. *Journal of Geophysical Research: Oceans*, *129*, e2023JC020369. https://doi.org/10.1029/2023JC020369

Received 14 AUG 2023
Accepted 10 DEC 2023

Abstract The Salish Sea is a large, fjordal estuarine system opening onto the northeast Pacific Ocean. It develops a strong estuarine exchange flow that draws in nutrients from the ocean and flushes the system on timescales of several months. It is difficult to apply existing dynamical theories of estuarine circulation there because of the extreme bathymetric complexity. A realistic numerical model of the system was manipulated to have stronger and weaker tides to explore the sensitivity of the exchange flow to tides. This sensitivity was explored over two timescales: annual means and the spring-neap. Two theories for the estuarine exchange flow are: (a) "gravitational circulation" where exchange is driven by the baroclinic pressure gradient due to along-channel salinity variation, and (b) "tidal pumping" where tidal advection combined with flow separation forces the exchange. Past observations suggested gravitational circulation was of leading importance in the Salish Sea. We find here that the exchange flow increases with stronger tides, particularly in annual averages, suggesting it is controlled by tidal pumping. However, the landward salt transport due to the exchange flow decreases with stronger tides because greater mixing decreases the salinity difference between incoming and outgoing water. These results may be characteristic of estuarine systems that have rough topography and strong tides.

Plain Language Summary The circulation of water in Salish Sea flushes the system with ocean water over a few months, much faster than could be explained by rivers alone. This flushing, or "exchange flow," is important because it brings in ocean nutrients to grow phytoplankton, and because it removes pollution. To understand why the exchange flow is as big as it is we analyzed the results of a realistic computer simulation. We found that tidal currents were important, but in competing ways. Stronger tides generally enhanced the exchange of water by forcing tidal eddies at places like sills. However stronger tides also increased vertical mixing, so the water in the eddies was just stirring the same water back and forth, instead of systematically bringing in ocean water and sending out river water.

1. Introduction

Estuaries are embayments connected to the ocean which have a source of buoyancy, usually one or more rivers, and a source of mixing, usually turbulence generated by tidal currents. The pattern of circulation that emerges from these ingredients tends to enhance the exchange of water between the estuary and the ocean (Bowen & Geyer, 2003; Hansen & Rattray, 1965; Lerczak et al., 2006). The fact that there is landward transport as part of this exchange, usually in the deeper part of the water column, has important biogeochemical consequences, including high primary production (Cloern et al., 2014) and organic particle remineralization (Dürr et al., 2011; Najjar et al., 2018). Although the details are different in each system, the key process is that sinking organic particles, and hence the nutrients they become via remineralization, are persistently swept back into the estuary in the deep landward flow, making them available for more than a single instance of primary production. These biogeochemical effects motivate the study of the estuarine exchange flow, however it is important to realize that it is not the exchange flow itself that is important, but rather its ability to exchange tracers with the ocean. This ends up being especially important in this paper because we find that the exchange flow in the Salish Sea increases with stronger tides but the salt transport due to the exchange flow decreases with stronger tides. This result is surprising in the context of two main theoretical models of the estuarine exchange flow. The first of these is "gravitational circulation" in which the baroclinic pressure gradient due to the along-channel salinity gradient drives persistent landward transport in deeper water, while the transport is limited by tidally driven turbulence. The second is "tidal pumping" in which tidal currents themselves drive the transport. These theories are described in greater detail below.

Considering the estuarine exchange flow in the context of a salt budget we may write:

$$\frac{d}{dt}\langle \int s\, dV \rangle = Q_{in} S_{in} + Q_{out} S_{out} \tag{1}$$

here the rate of change of tidally averaged (angle brackets) net salt in the estuary volume, V, landward of some section equals the transport of salt through the section. Here we write the tidally averaged transport through the section as occurring in two layers with volume transports Q_{in}, Q_{out} [$m^3 s^{-1}$] and transport-weighted salinities S_{in}, S_{out} [g kg^{-1}]. These are calculated in this paper using the Total Exchange Flow (TEF) method (Burchard et al., 2018; Lorenz et al., 2019; MacCready, 2011). Subscript "out" means out of the estuarine volume, and the sign convention is that Q_{out} is negative, while Q_{in}, and Q_R, the river volume transport, are positive. Volume conservation, neglecting changes in the volume, is expressed as:

$$Q_{in} + Q_{out} + Q_R = 0 \tag{2}$$

The salinity difference between in- and out-flowing layers is:

$$\Delta S = S_{in} - S_{out} \tag{3}$$

Rewriting Equation 1 using Equations 2 and 3 gives the final form of the salt budget:

$$\frac{d}{dt}\langle \int s\, dV \rangle = Q_{in} \Delta S - Q_R S_{out} \tag{4}$$

as used in Broatch and MacCready (2022). The physical meaning of the terms on the right hand side of Equation 4 are (a) the inward salt transport due to the exchange flow, and (b) the outward salt transport associated with the river flow.

TEF is only one of several estuarine salt flux decompositions we could have used (Chen et al., 2012; Garcia & Geyer, 2023; Geyer & MacCready, 2014; Lemagie et al., 2022). The advantage of TEF, especially in the budget (4), is that it allows separate consideration of the exchange flow, here taken as synonymous with Q_{in}, and the salinity difference it acts on, ΔS. Chen et al. (2012) used this decomposition to show that Q_{in} scaled with $\partial s/\partial x$ in the Hudson River, an estuary where the salt intrusion is long compared to the tidal excursion. In contrast, Chen et al. (2012) found that for the Merrimack River, a "short" estuary that has a length comparable to the tidal excursion, Q_{in} scaled with tidal transport, especially near the mouth. Chen et al. (2012) concluded that a jet-sink mechanism (Stommel & Farmer, 1952) in the short estuary was causing the water that entered on flood to be different from what left on ebb, an example of tidal pumping. One result of the analysis presented here is that this "short estuary" scaling can also apply in a much larger system like the Salish Sea, owing to several constrictions at energetic sills.

There has been significant past work on scaling in the long estuary case, as reviewed in MacCready and Geyer (2010). This theory can be called gravitational circulation. In this theory the exchange flow is forced by a baroclinic pressure gradient due to the along-channel salinity gradient, $\partial s/\partial x$, and opposed by turbulent shear stress. For scaling purposes, we will use K for both the vertical eddy viscosity and eddy diffusivity. It is often observed in estuaries that the vertical eddy viscosity and diffusivity are proportional to the amplitude of the tidal velocity (Chant & Wilson, 2000; Giddings et al., 2011; Peters & Bokhorst, 2001) which is to be expected because the tidal velocity is typically an order of magnitude greater than the tidally averaged velocity, and in estuaries the thickness of the bottom boundary layer is often a significant fraction of the water depth. The eddy viscosity also tends to increase when there is less vertical density stratification, which makes more precise scaling of K significantly more complicated than presented here. Nonetheless, the sign of the influence is consistent: stronger tides mix more, decreasing stratification, leading to more mixing. A convenient way to quantify the strength of tides at a given section is by the amplitude of the tidal velocity, U_T. This would vary over the spring-neap cycle, and to a first approximation K would be expected to vary linearly with U_T (Geyer et al., 2000). The scaling for the exchange flow due to gravitational circulation is:

$$Q_{in} \propto A U_{in} = Ag\beta H\left(H^2/K\right)\partial s/\partial x \tag{5}$$

here $g = 9.8$ [m s^{-2}] is gravity, $\beta = 7.7 \times 10^{-4}$ relates density, ρ, to salinity in a linear equation of state, $\rho = \rho_0(1 + \beta s)$, and $\rho_0 = 1{,}000$ [kg m^{-3}] is the density of freshwater. H is the channel depth and A is the cross-sectional area. Vertical stratification is created by the exchange flow straining $\partial s/\partial x$, and reduced by vertical mixing due to vertical eddy diffusivity, K (we assume eddy viscosity and eddy diffusivity are the same within a constant of proportionality). The scaling for the stratification is:

$$\Delta S \propto U_{in}\partial s/\partial x\left(H^2/K\right) = g\beta H(\partial s/\partial x)^2\left(H^2/K\right)^2 \tag{6}$$

There are two timescales to consider with these scaling relations. For timescales that are too short for $\partial s/\partial x$ to adjust to changing K, that is, shorter than the "adjustment time" (Lerczak et al., 2009), Equations 5 and 6 predict that $Q_{in} \propto K^{-1}$ and $\Delta S \propto K^{-2}$. It is often observed that these do both decrease markedly during spring tides (Aristizábal & Chant, 2015; Geyer & Cannon, 1982; Giddings et al., 2011; Haas, 1977; Jay & Smith, 1990; Ralston et al., 2008). For timescales longer than the adjustment time $\partial s/\partial x$ changes as well, scaling as K, and the predicted steady scaling relations for gravitational circulation are:

$$Q_{in} \propto Ac(U_R/c)^{\frac{1}{3}} \tag{7}$$

and

$$\Delta S \propto S_{ocn}(U_R/c)^{\frac{2}{3}} \tag{8}$$

as reviewed in MacCready and Geyer (2010). Here $c = (g\beta S_{ocn}H)^{1/2}$ is the maximum possible two-layer intrusion speed for seawater with salinity S_{ocn} flowing under freshwater. The speed associated with river flow is $U_R = Q_R/A$. Notably, these long-term, steady scaling relations (7) and (8) predict no sensitivity at all to K.

The general expectation from the scaling results presented above for estuaries dominated by gravitational circulation is that both Q_{in} and ΔS will decrease with stronger tides over short time scales. These will lead to the system losing salt, and over long time scales will result in a shorter salt intrusion length. However, in many estuaries the primary physics governing the landward salt transport is not gravitational circulation, but instead some form of tidal pumping (Aristizábal & Chant, 2015; Banas et al., 2004; Becker et al., 2009; Garcia & Geyer, 2023; Giddings et al., 2011; Stigebrandt, 1976; Wang et al., 2015; Whitney et al., 2016), particularly near the mouth (Aristizábal & Chant, 2013; Fram et al., 2007; Hughes & Rattray, 1980; Xiong et al., 2021). A review of mechanisms is given in MacCready and Banas (2011), and a review in the context of fjords is given in Farmer and Freeland (1983). As mentioned above, Chen et al. (2012) compared the exchange transport Q_{in} in two modeled estuaries to the maximum possible exchange that could be achieved by tides. The maximum tidal exchange would occur if all the water going seaward on ebb had a different salinity than all the water entering on flood. Chen et al. (2012) define this as:

$$Q_{prism} \equiv \frac{1}{T}\int_0^{T/2} Q_T \sin(\omega t)\, dt = \frac{Q_T}{\pi} \tag{9}$$

where T is the tidal period, and we have assumed $Q_R \ll Q_T$ and $Q_T = AU_T$. They found that in an estuary whose length was comparable to the tidal excursion the exchange flow did not scale like gravitational circulation (5) but instead was very well described by a tidal pumping scaling of the form:

$$Q_{in} \propto Q_{prism} \tag{10}$$

For their example of the Merrimack River they found a relatively efficient scaling constant of 0.65 and attribute it to a jet-ink asymmetry near the mouth, as hypothesized in Stommel and Farmer (1952). Chen et al. (2012) did not address the scaling of ΔS. Here we hypothesize that ΔS increases with tides, at least for spring-neap variation, because the greater tidal excursion can access a greater range of the along-channel salinity gradient. The landward salt transport in the tidal pumping case has historically been expressed as the product of section area times some large along-channel diffusivity, K_H, times the salinity gradient, $\partial s/\partial x$, with K_H being proportional to the tidal velocity (Banas et al., 2004) and a length scale that may be set by bathymetry (a "mixing length" argument). While one can always find a value of K_H that satisfies $AK_H\partial s/\partial x = Q_{in}\Delta S$ there is no direct way, aside from making the TEF decomposition, to know what the individual values of Q_{in} and ΔS might be even if you know

(a)	Gravitational	Tidal Pumping
Spring-Neap variation of U_T $\partial s/\partial x$ constant	$Q_{in} \propto \frac{1}{U_T}, \Delta S \propto \frac{1}{U_T^2}$	$Q_{in} \propto U_T, \Delta S \propto U_T$
Equilibrated	$\partial s/\partial x \propto U_T$ Q_{in} and ΔS constant at mouth	$\partial s/\partial x \propto 1/U_T$ $Q_{in} \propto U_T, \Delta S \propto \frac{1}{U_T}$

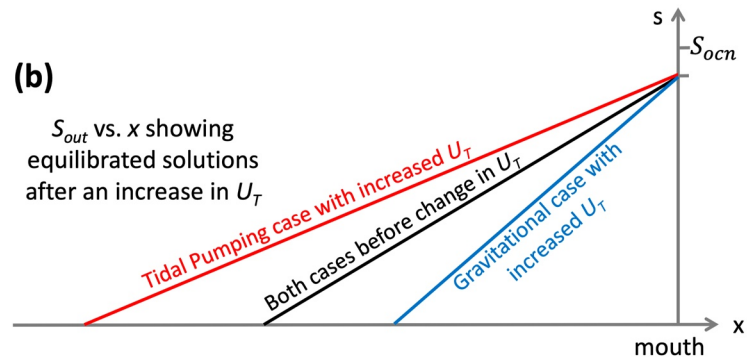

Figure 1. Scaling expectations (a) for variation of Q_{in} and ΔS due to changes in the amplitude of the tidal current U_T. The expectations are shown under the assumption that the salt transport is controlled by either gravitational circulation or tidal pumping. Two time scales are considered. For spring-neap variation of U_T it is assumed that the variation is faster than the adjustment time and so $\partial s/\partial x$ is taken as constant. For long time scales we assume $\partial s/\partial x$ adjusts to the new value of U_T as shown in (b).

their product. For longer time scales over which the steady version of Equation 4 is applicable we expect ΔS to be governed by:

$$\Delta S = Q_R \frac{S_{out}}{Q_{in}} \tag{11}$$

which is just a rearrangement of the steady Knudsen Relation (Burchard et al., 2018).

In Figure 1, we summarize the scaling expectations given above, assuming that the amplitude of the tidal velocity at a section, U_T, can be taken to be proportional to the vertical eddy viscosity and diffusivity, K, and to Q_{prism}. Expectations are given assuming the dynamics are either gravitational or tidal pumping, and for short (spring-neap) and long (equilibrated) time scales. These expectations will serve as a rough guide to our interpretation of the numerical experiments.

In the remainder of this paper, we explore the dynamical response of transport through many sections in a realistic model of the Salish Sea, evaluating them in the context of these scaling relations. We find that the tidal pumping scaling (10) is unexpectedly good at predicting Q_{in} throughout the system for long time scales. The scaling for ΔS is much more consistent with gravitational circulation (6), even though it may not be created by gravitational circulation.

The Salish Sea, Figure 2b, is a complex system compared to better-understood estuaries like the Hudson River (Ebbesmeyer et al., 1988; LeBlond, 1983). It has many separate branches, and deep, wide basins with weak tidal currents punctuated by shallow, narrow sills that can have tidal currents over 4 m s^{-1}. The tides here are mixed-semidiurnal and have large amplitude: over 6 m range in some places for a perigean spring tide around the solstices (Mofjeld & Larsen, 1984). Rivers enter at many locations, with the biggest ones, the Fraser and Skagit Rivers, far from the heads of the channels (Figure 2c). The magnitude of the exchange flow in the Salish Sea has been estimated using Knudsen's relation combined with observations of the salinity field (Cokelet et al., 1991; Mackas & Harrison, 1997), and occasionally from current meters (Bretschneider et al., 1985; Cannon

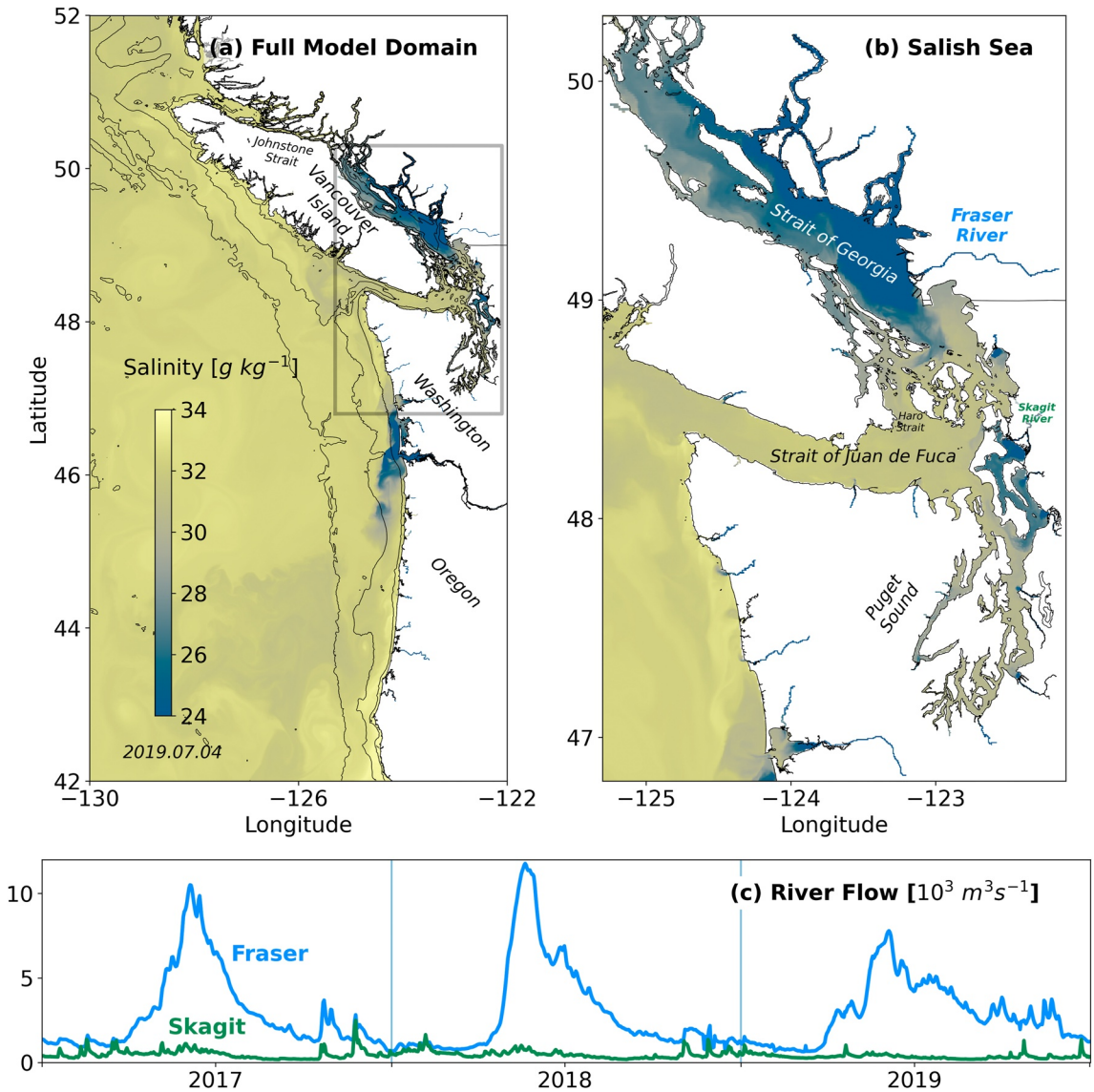

Figure 2. LiveOcean model domain (a) with surface salinity from 4 July 2019. A close-up of the model in the Salish Sea is plotted in (b). Time series for the two largest rivers entering the Strait of Georgia and Puget Sound are plotted in (c).

et al., 1979; Thomson & Huggett, 1980; Thomson et al., 2007). The dynamical balance governing the exchange flow in the Strait of Juan de Fuca has been evaluated in model analyses (Giddings & MacCready, 2017; Martin & MacCready, 2011) and been found to be influenced by a combination of tides, winds, rivers, and gravitational circulation. At the south end of Admiralty Inlet, the seaward entrance to Puget Sound, moored time series clearly showed that the exchange flow and stratification increased at neap tides (Geyer & Cannon, 1982), at least when measured at a single mooring. There is also good observational evidence that the densest water flows landward over Admiralty Inlet during apogean neap tides (Deppe et al., 2018). Other things we know about the system response (MacCready et al., 2021) are that during seasons or years of low river flow the mean salinity increases and ΔS decreases. There is some evidence that Q_{in} increases weakly with Q_R seasonally, but little evidence that there is much difference in mean Q_{in} between wet and dry years. More study is required to establish the adjustment time and sensitivity to changes in river flow. For the Salish Sea as a whole there is no consensus about dynamical controls over the exchange flow or the salt transport due to the exchange flow, motivating this study.

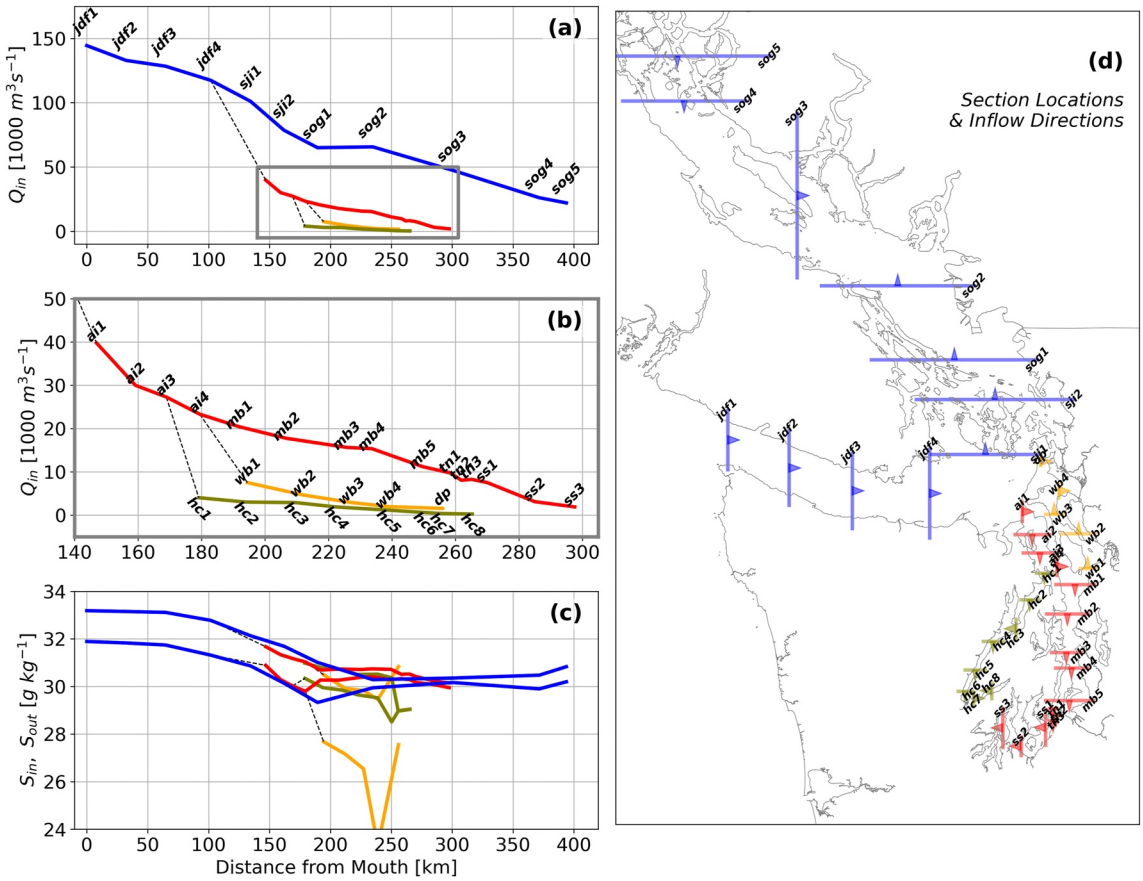

Figure 3. Annual mean TEF Q_{in} for 2018 (a) at sections throughout the Salish Sea. Section locations and inflow direction are plotted in (d). A close-up of the transports for Puget Sound is plotted in (b). Annual mean S_{in} and S_{out} for the sections is plotted in (c). The sections names help identify various parts of the system: **jdf** for the Strait of Juan de Fuca, **sog** for the Strait of Georgia, **sji** for the San Juan Islands, **ai** for Admiralty Inlet, **mb** for Main Basin, **tn** for Tacoma Narrows, **ss** for South Sound, **hc** for Hood Canal, **wb** for Whidbey Basin, and **dp** for Deception Pass.

2. Methods

We use a realistic numerical simulation of the Salish Sea and regional coastal ocean, Figure 2a. The model, LiveOcean, has been previously described and evaluated against observations in MacCready et al. (2021); see in particular the Supplement to that paper. The model has 500 m horizontal resolution in most of the Salish Sea, 30 terrain-following vertical levels, and uses the ROMS (Regional Ocean Modeling System) code framework. It is forced by realistic wind stress and atmospheric heat fluxes, rivers, tides, and open ocean boundary conditions. The run used here was initialized on 15 December 2016, and run as a hindcast for over 6 years. We use the year 2018 for this case study because (a) this gives ample time for the model to equilibrate from any initial condition imbalances, and (b) 2018 was a relatively ordinary year in terms of forcing. To explore the system sensitivity to tidal forcing we also ran two modified versions of the 2018 model year. In one case the amplitude of all tidal forcing at the open ocean boundaries was decreased to be 75% of the original. In the other case the tidal forcing was increased to be 110% of the original. All other forcing was unchanged, and all models were initiated from the same state on 1 January 2018. We tried to run with 125% of the tidal forcing, but the model was unstable with any time step that could be run in a reasonable amount of time.

The tidally averaged exchange flow was evaluated over the year 2018 in the three model runs using the Total Exchange Flow method at 39 sections (Figure 3d). These are analyzed as time-series, and as full-year averages, to understand the system response to (a) spring-neap variation of U_T and (b) the equilibrated response to the changed tidal forcing.

The TEF method, in which salt transport through a section is first binned by salinity before tidal averaging (MacCready, 2011), is a good way of finding out what the size of $Q_{in}\Delta S$ and it two constituent parts are. TEF

alone provides no information on why the values of Q_{in} and ΔS have the values they do, but when combined with the variation of the strength of the tidal transport, Q_{prism}, we arrive at a conceptual model of the Salish Sea in which tidal pumping is critical for forcing Q_{in}, but in which the inevitability of more mixing, and hence decreased ΔS, with stronger tides more than compensates for the increased Q_{in}.

3. Results

The spatial pattern of along-channel variation of annual average Q_{in} for the original run is shown in Figure 3a, with a close-up of the Puget Sound channels in Figure 3b. The spatial pattern of S_{in} and S_{out} is plotted in Figure 3c. As discussed in MacCready et al. (2021) the overall pattern has a large exchange flow at the mouth, the western end of the Strait of Juan de Fuca, that decreases relatively smoothly going landward, despite extreme differences in tidal flow speed and depth between sills and basins. The salinity also decreases going landward, but with weak gradients and small ΔS, implying that the natural length of the salt intrusion is many times greater than the physical length of the bathymetry. In this paper we seek to understand the physical controls on the fields in Figure 3. Are they best described using the theory of gravitational circulation, or the theory of tidal pumping, or something else? Our analysis is structured around the expected responses of Q_{in}, ΔS, and $\partial s/\partial x$ summarized in Figure 1. Where possible we look for matches to predicted scaling, for example, does the spring-neap variation of Q_{in} go like U_T^{-1}? But in a complex system like the Salish Sea we find that understanding requires a less refined approach, for example, does Q_{in} increase or decrease with U_T?

3.1. Spring-Neap Variation

A year-long salt budget for the original run is shown in Figure 4a, using the terms presented in Equation 4. Because the system volume is not constant with time, we use a more complete version of volume conservation (2) and define the "adjusted Storage" as

$$Storage^{adj} = \frac{d}{dt}\langle \int s\, dV \rangle - \frac{dV}{dt} S_{out} \tag{12}$$

This smooths out high-frequency noise in the storage term in Equation 4 and is required for a closed budget. The small error term in Figure 4a is the residual of the sum of all budget terms and is non-zero because of approximations such as using hourly snapshots for the calculation of TEF transports. The salt budget shown is for the Puget Sound volume bounded by sections **ai1** at the north end of Admiralty Inlet, and **dp** at Deception Pass in the north end of Whidbey Basin. We have computed similar budgets for other sub-basins, and for the entire Salish Sea; there are similarities but also differences that are explored in the analysis below. The budget shows that the volume is losing salt during large river flow events in the winter, and gradually gaining salt during the summer period of low river flow. We focus our attention on the summer period, July through October because spring-neap variability is clearest, and not obscured by big river or wind events.

The panels (b)–(d) in Figure 4 are time series focusing on the terms in the landward salt transport due to the exchange flow, $Q_{in}\Delta S$. In each there is an additional line for the strength of the tidal transport, Q_{prism}, which is high at spring tides and low at neap tides. In Figure 4b it is apparent that $Q_{in}\Delta S$ is high during neap tides, especially apogean neaps (the lower lows of Q_{prism}). The same is true of ΔS, Figure 4d. However, Q_{in} increases at spring tides, Figure 4c. The proportional variation of ΔS is greater, thereby controlling the salt transport. The variation of Q_{in} versus Q_{prism} is consistent with our expectations for tidal pumping, but the result is surprising because in observations at the Admiralty Inlet sill Geyer and Cannon (1982) found that the exchange flow was decreased at spring tide. The reason for this discrepancy is that in Figures 4b–4d the time series are plotted at the north end of Admiralty Inlet, whereas the (Geyer & Cannon, 1982) observations were made near the south end, near section **ai4**, discussed below.

Time series from the standard run for the months July through October are presented as property-property plots for four sections in Figure 5. These four sections were selected because they are at energetic sills that potentially control the system-wide exchange. Several different behaviors are evident. For section **ai1** at the north end of Admiralty Inlet we can see a hybrid of the spring-neap scaling expectations from Figure 1. While ΔS follows the Q_{prism}^{-2} scaling expected of gravitational circulation (Figure 5c), Q_{in} varies as Q_{prism}, consistent with tidal pumping, although the slope appears to be flattening out at neap tides (Figure 5b). In contrast, at the southern end

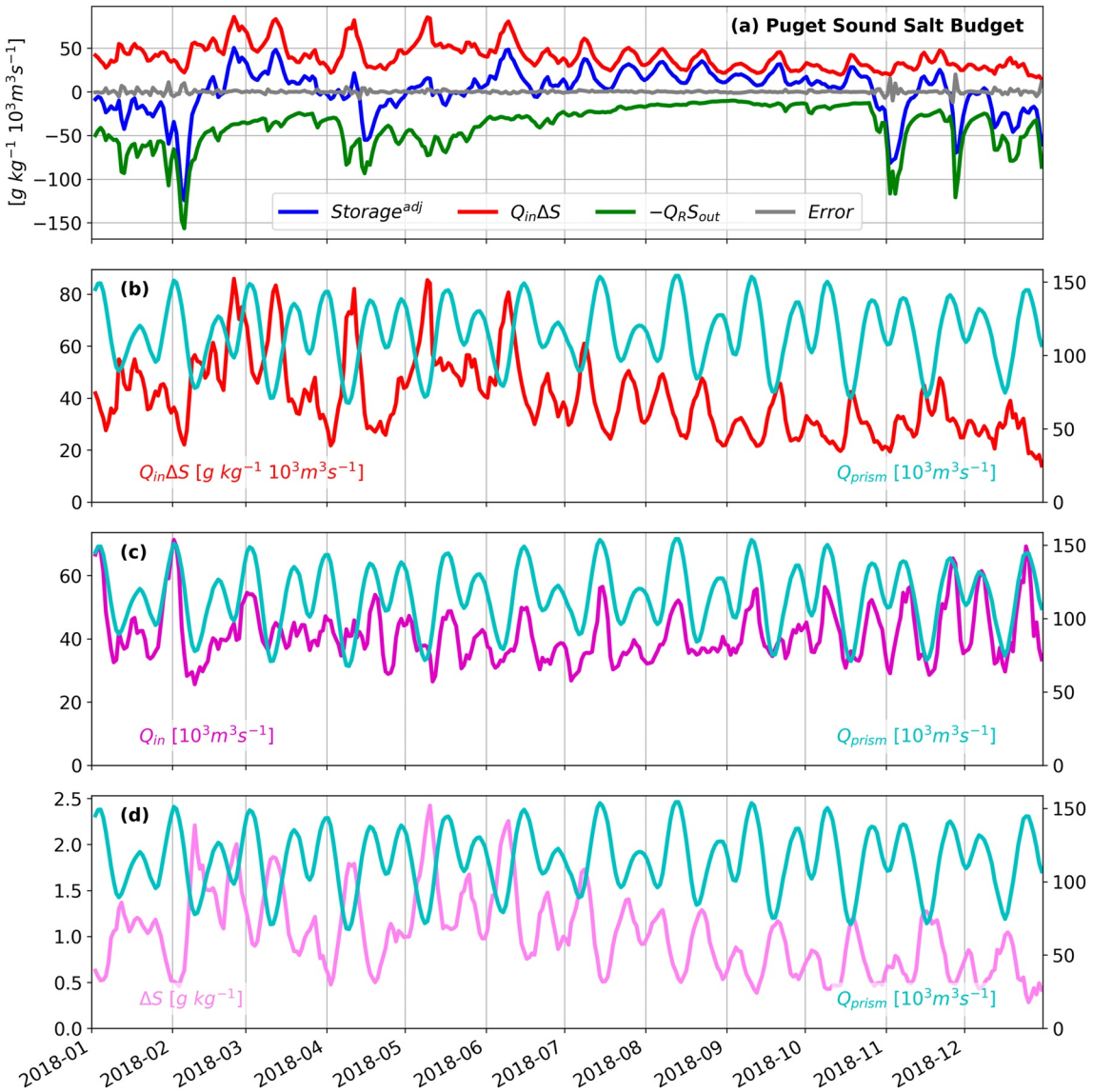

Figure 4. Time series for tidally averaged terms in a salt budget are plotted in (a) for the Puget Sound volume bounded by sections **ai1** and **dp**. The terms are defined in Equations 4 and 12. Panels (b)–(d) show time series of $Q_{in}\Delta S$, Q_{in}, and ΔS for the sum of the bounding sections (the signals are dominated by **ai1**). For reference in identifying times of spring and neap tides Q_{prism} is plotted as a cyan line in (b)–(d) with its scale given on the right hand of each panel.

of the Admiralty Inlet sill, Q_{in} for section **ai4** scales more like Q_{prism}^{-1}, as expected for gravitational circulation, although the slope appears to be flattening at spring tides. For both sections the product, $Q_{in}\Delta S$, Figure 5d, indicates less landward salt transport during spring tides, although not decreasing as much as the expectations from gravitational scaling would suggest. The proportional change in ΔS dominates whatever change occurs in Q_{in}. A different pattern is evident at section **tn2**, situated in the highly energetic Tacoma Narrows region to the south. This constriction can have a tidal excursion that exceeds the sill length, and because of channel curvature it can overturn the water column, causing intense mixing (Seim & Gregg, 1997). The result is that Q_{in} behaves strongly like tidal pumping, ΔS has no clear pattern, and the salt transport increases with Q_{prism}. A final example is the section **sji1**, at the southern edge of the San Juan Islands, a complex archipelago that separates the Strait of Juan de Fuca from the Strait of Georgia. There are several deep, energetic channels on this section, the biggest of which is Haro Strait on the west (Pawlowicz, 2002). Here the patterns are like a messy version of those at Admiralty Inlet, and the result is that salt transport does not have a clear relation to the tides.

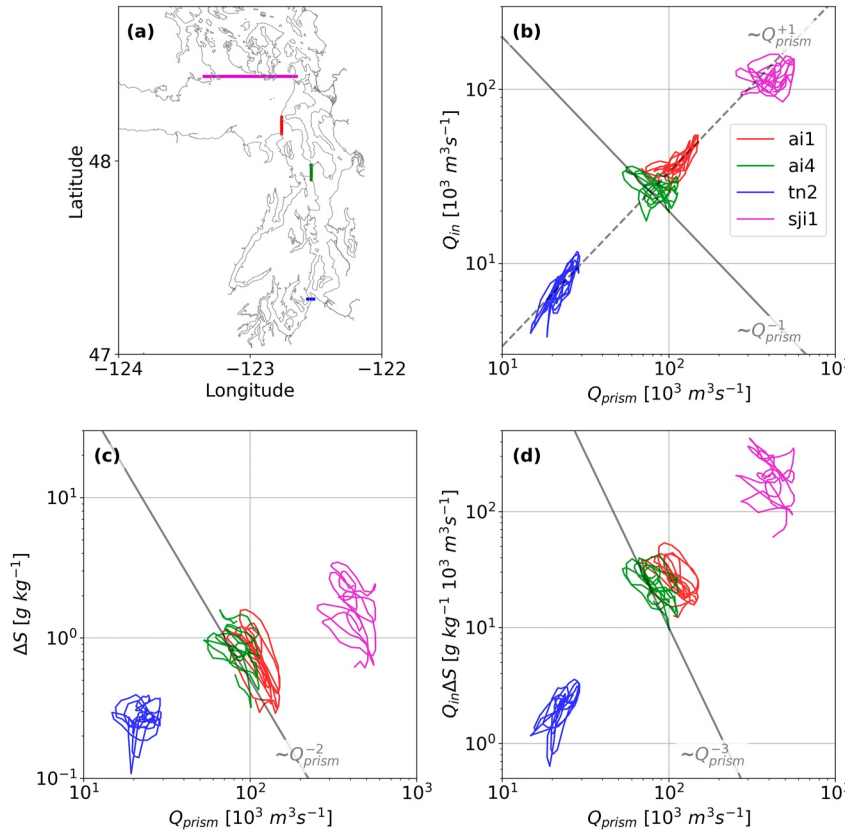

Figure 5. Time series property-property plots over the months July-October 2018 at four sections with locations plotted in (a). Sections **ai1** and **ai4** are at the north and south ends of Admiralty Inlet, respectively. Section **tn2** is in Tacoma Narrows, the sill separating Main Basin of Puget Sound from South Sound. Section **sji1** crosses several passes through the San Juan Islands, and is the primary connection to the ocean for the Strait of Georgia to the north. The property-property plots show (b) Q_{in}, (c) ΔS, and (d) $Q_{in}\Delta S$, all versus Q_{prism}, with log-log axes. Lines representing the slopes of various scaling expectations are included. The individual "scribble" for each section is centered at a different place on the x-axis because of the large spatial variation of Q_{prism}.

Because of its importance to gravitational circulation, we look in more detail at $\partial s/\partial x$. In Figure 6 we plot time series of tidally averaged salinity on six sections along Admiralty Inlet. At each section the hourly salinity has been extracted, sorted by z-position, tidally averaged, and then only z-levels existing at all six sections are retained. In Figure 6b we plot the vertical profiles for all sections at a selected neap (solid lines) and spring (dashed lines) tide. The time series of depth means are plotted in Figure 6c, and end-to-end $\partial s/\partial x$ is plotted as a time-series in Figure 6d. Contrary to the expectations laid out in the Introduction and Figure 1, the salinity gradient has some variation with the spring-neap cycle, becoming weaker during spring tides. This may be because enhanced mixing by headland eddies homogenizes the along channel salinity structure more during spring tides than neap. This variation of $\partial s/\partial x$ would be expected to amplify the gravitational circulation responses to tidal velocity given in Equations 5 and 6. However, the relative variation of $\partial s/\partial x$ in the late summer is only about 30%, whereas the relative variation in the strength of the tidal transport, Q_{prism}, is more like 100% (Figure 6d), so we expect that the variation of $\partial s/\partial x$ is not of leading importance.

3.2. Equilibrated Results

Taking the annual-average of the TEF properties at all our sills we may explore the spatial patterns and bring in the results of our strong and weak tide manipulation experiments. Taking the annual mean gives results that are equivalent to looking at the system over time scales long enough for $\partial s/\partial x$ to adjust to the forcing (Chen, 2017; MacCready, 2007). The adjustment time has not been rigorously explored in the Salish Sea, but it is likely shorter

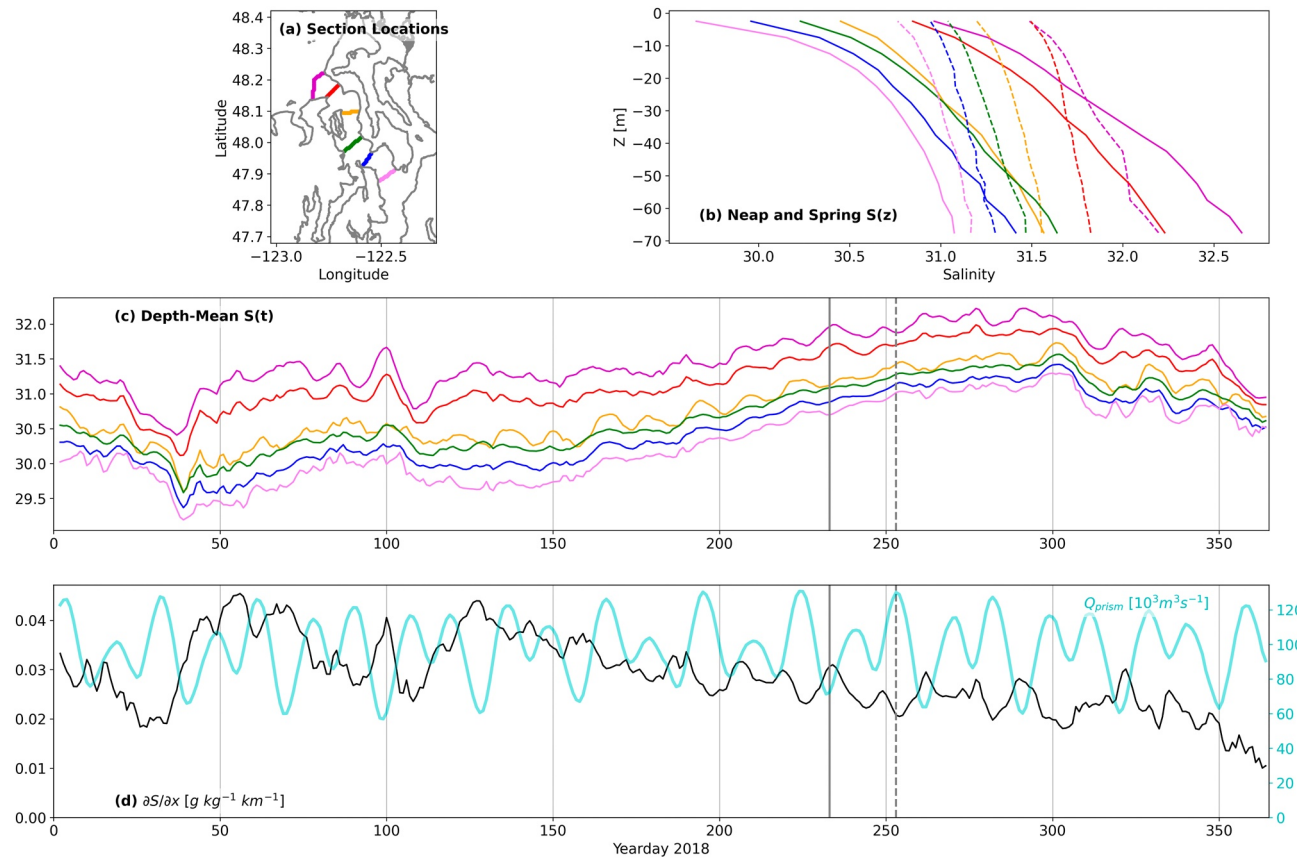

Figure 6. Tidally averaged salinity for the year 2018 at 6 sections along Admiralty Inlet shown in (a). Snapshots at neap (solid) and spring (dashed) tides for $S(z)$ are plotted in (b). Time series of depth-mean $S(t)$ at all section are plotted in (c). A time series of $\partial S/dx$ calculated from depth-mean salinity from the most seaward to the most landward section is plotted in (d), with a time series of Q_{prism} for reference. The overall length of the sill is 41 km.

than the residence time, which is months to a year (MacCready et al., 2021). The longer times are due to the large volume of the Strait of Georgia.

Annual means for Q_{in} versus Q_{prism} at all sections, and for all three tide-manipulation experiments, are plotted in Figure 7. There is a striking pattern to the results: over three orders of magnitude $Q_{in} \propto Q_{prism}$, with a constant of proportionality of about 1/3.5. Thus, the overall exchange flow behavior is consistent with tidal pumping. This result was entirely unexpected. The results for ΔS, shown in Figure 8, are consistent with the steady Knudsen Relation (11) as they must be: we expect $\Delta S = Q_R S_{out}/Q_{in} \propto Q_R S_{out}/Q_{prism}$ and this Q_{prism}^{-1} pattern is evident in Figure 9. Note that these do not all collapse onto a single line because of the different river flow experienced by each section (variation of S_{out} is generally much smaller than the variation of Q_R).

The net effect of our manipulation of the tides can be seen in time series of volume-mean salinity in different volumes of the system, Figure 9. In all four volumes the salinity decreases for stronger tides. We may conclude that $Q_{in}\Delta S$ also decreases with stronger tides despite the results in Figure 7 that in most cases Q_{in} increases. The proportionally greater decrease of ΔS apparently wins out, at least at enough controlling sections to define the overall system response. The results for Puget Sound are to be expected given our results for **ai1** and **ai4** in the scribble plots in Figure 5d. The South Sound volume also grows fresher with stronger tides even though section **tn2** is at its mouth and this section showed $Q_{in}\Delta S$ increasing with Q_{prism}. The reason is that Main Basin salinity was decreased because of the limitation at Admiralty Inlet or Juan de Fuca, and thus the salinity presented at the mouth of South Sound was decreased. We may also judge equilibration times from the "75% minus 110%" filled areas at the bottom of the panels in Figure 9. Approximate equilibration is reached after 3 months in the sub-basins but takes more like 7 months for the Salish Sea volume (a) which is influenced by the large volume of the Strait of Georgia.

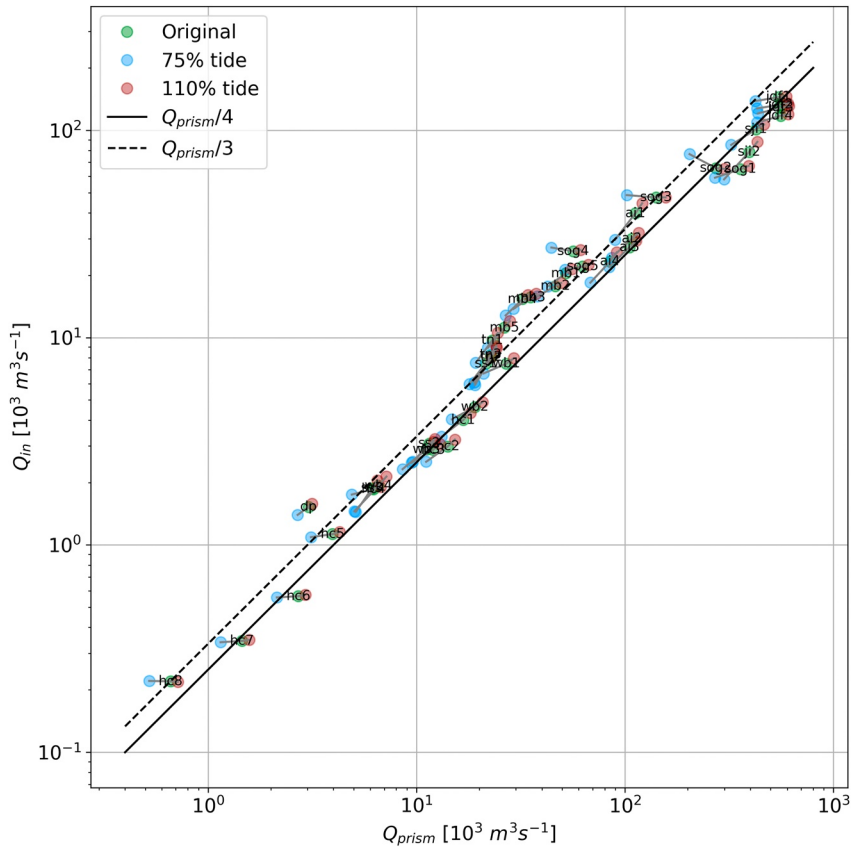

Figure 7. Annual mean Q_{in} versus Q_{prism} for all the sections shown in Figure 3d. For each section the results of three experiments with varying tidal strength are shown in different colors, connected by a short line. Lines for $Q_{prism}/4$ and $Q_{prism}/3$ are plotted for reference.

4. Discussion

The results presented above emphasize the importance of $Q_{in}\Delta S$ as a more fundamental quantification of the exchange flow than Q_{in} alone. Here we explore both quantities, system-wide. In Figure 10 we summarize how Q_{in} responds to variation of tide strength over spring-neap (Figure 10a) and annual mean (Figure 10b) timescales, at all the TEF sections. In both panels the circle size is proportional to the magnitude of $(\partial Q_{in}/\partial Q_{prism}) \times \overline{Q_{prism}}^{t}$ where $\overline{Q_{prism}}^{t}$ is the time average of Q_{prism} over either four-month (a) or annual (b) periods. For spring-neap variation the response is calculated as the slope of a line fit through a property-property time series like those plotted in Figure 5b. For the annual timescale (equilibrated) the slope is calculated from the difference of the annual means of the 110% and 75% tide manipulation experiments. Positive slope is red, meaning Q_{in} increases with Q_{prism}, and blue is negative, meaning it decreases. From the line fit used for the spring-neap variation we can also calculate a correlation coefficient, and the magnitude of this is proportional to the opacity of the circles in Figure 10a. Stronger correlation is more opaque. The spring-neap response (Figure 10a) is highly variable throughout the system, with positive slope (like tidal pumping) mostly associated with energetic sills like Admiralty Inlet (but only at the north end), Tacoma Narrows, Deception Pass, the San Juan Islands, and Johnstone Strait. The deeper basins and the Strait of Juan de Fuca generally show negative slope and smaller correlation coefficients. In contrast, almost all sections show positive slope when considering annual means from the tide manipulation experiments (Figure 10b). The difference between the two timescales likely is evidence of the requirements of continuity: the transport at the sills controls the transport between the sills over longer timescales, whereas for shorter timescales the response can be more localized. We will assume that the energetic sills with clear patterns (high correlation coefficient) control the overall behavior of the Salish Sea, and that the basins between them are merely passive conveyors that interpolate across their bounding

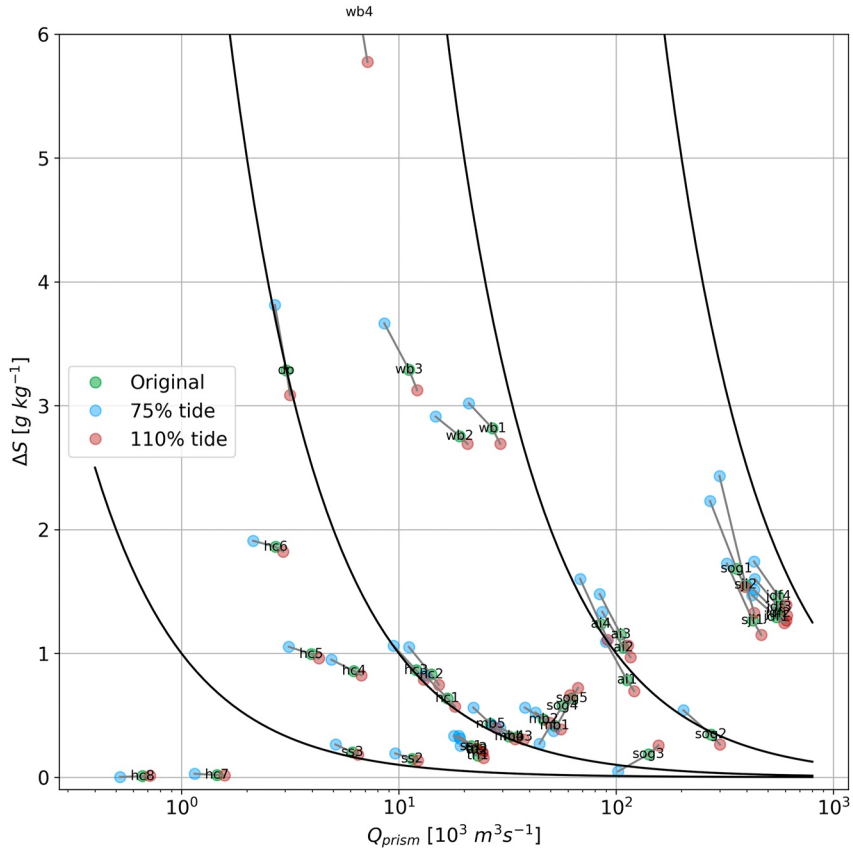

Figure 8. Annual mean ΔS versus Q_{prism} for all the sections shown in Figure 3d. For each section the results of three experiments with varying tidal strength are shown in different colors, connected by a short line. Several lines proportional to Q_{prism}^{-1} are plotted for reference.

sills, smoothing the differences. Their great depth allows rapid gravitational adjustment. We stress that this assumption is not proven in our analysis. There is no rigorous definition of "control" except in simple cases where steady hydraulic theory can be applied. Hydraulic theory with continuous stratification was applied to observations on sections over the sill in Hood Canal (Gregg & Pratt, 2010) who concluded "Full interpretation exceeds observations and existing theories".

Clearly, even though Q_{in} generally increases with stronger tides in the Salish Sea for annual mean timescales, this increase does not translate to more salt being brought into the system, in fact it is the opposite (Figure 9). In Figure 11 we summarize results of how $Q_{in}\Delta S$ responds to tides for all sections for spring-neap (Figure 11a) and annual (Figure 11b) timescales. Figure 11 is identical in construction to Figure 10, except that the quantity being considered is $Q_{in}\Delta S$ instead of Q_{in}. For both timescales the variation of $Q_{in}\Delta S$ is generally greater for the more seaward sections, reflecting the fact $Q_{in}\Delta S$ is also greater for more seaward sections. The spring-neap variation tends to be greater than the annual mean variation from the tide manipulation experiments (the circles in Figure 11a are bigger than in 11b). The sign of variation is mostly negative (blue circles) for the annual means, with notable exceptions in Whidbey Basin and northern Strait of Georgia. The results in Figure 9 demonstrate that these exceptions do not dominate the system response. The sign of spring-neap variation is more complicated, with eastern Juan de Fuca and Admiralty Inlet being negative and Tacoma Narrows being positive.

The system-wide tendency toward negative response ($Q_{in}\Delta S$ decreasing with stronger tides) indicates that the decrease of ΔS more than compensates for the increase of Q_{in}. One could think of this as the exchange flow becoming less "efficient" with stronger tides, exchanging more water that has less salinity difference. There are three things that affect the efficiency of the exchange flow and cause the salt transport to decrease with stronger tides despite the increase in Q_{in}. First is the change in stratification, second is the change in $\partial s/\partial x$, and

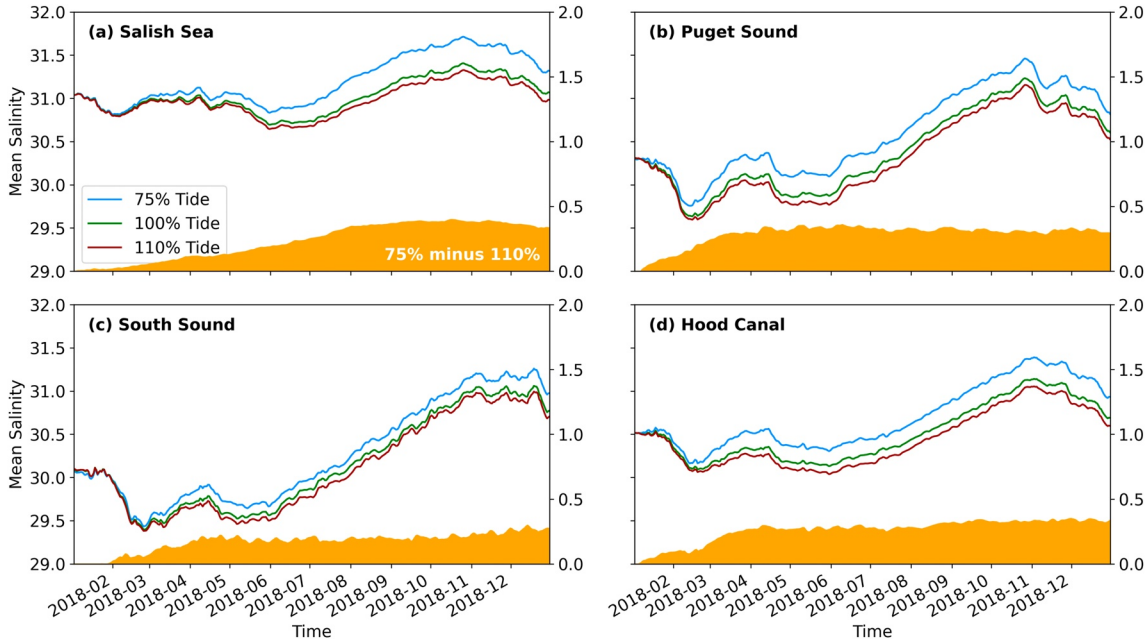

Figure 9. Time series of volume-mean salinity for the year 2018, for the three different tide strength experiments. Results for the entire Salish Sea volume are plotted in (a). Results for sub-volumes are plotted in (b)–(d) for Puget Sound, South Sound, and Hood Canal. In each panel the filled curve at the bottom shows the salinity difference between the 75% and 110% tide experiments, with the scale given at the right.

third is the change in the structure of the tidal flow: vertical and lateral shear as well as structure of eddies (Garcia & Geyer, 2023). The first two make efficiency go down and are both evident for Admiralty Inlet in Figure 6. The decrease in stratification and in $\partial s/\partial x$ are consistent with the decrease in ΔS. The effect of the structure of tidal flow is more complicated and can have positive and negative effects on exchange. Other studies (Geyer & Cannon, 1982; Geyer et al., 2000) have shown that there tends to be more mean vertical shear during neaps. This goes along with the change in $\partial s/\partial z$ and makes the exchange flow more efficient. This may be understood in terms of the switch in relative importance of the two separate mechanisms: sub-tidal shear flow versus tidal pumping.

This study puts some doubt on the importance of gravitational exchange flow in the Salish Sea. However, if we consider the driving force for the exchange flow when the salt flux is maximal, during neap tides (Figure 4), we may conclude that gravitational exchange flow is important, but because the long-term averaged exchange flow is volumetrically dominated by spring tides, it scales with the tidal prism.

5. Conclusions

The results and analysis presented here lead to a partial understanding of the dynamics of the estuarine exchange flow in the Salish Sea:

1. Expressing the landward salt transport using the TEF formulation as $Q_{in}\Delta S$ allows us to separately explore the exchange volume transport and the salinity difference it works on.
2. We find in annual averages that Q_{in} scales as approximately $0.3 \times Q_{prism}$ at sections throughout the system and over three orders of magnitude of Q_{prism}, the strength of the tidal transport.
3. Spring-neap variation of Q_{in} versus Q_{prism} at individual sections shows a richer set of responses, some matching the expectations of tidal pumping, some more consistent with gravitational circulation, and some with no clear signal.
4. In the tide manipulation experiments there is clear tendency for annual-averaged ΔS to decrease with stronger tides. This can be thought of as a requirement for a balanced salt budget when Q_{in} increases with stronger tides. While causality is hard to prove in this case, we hypothesize that the change in Q_{in} is forced by stronger tides (consistent with tidal pumping) and that ΔS responds as needed to maintain the landward salt transport to balance $Q_R S_{out}$ which has relatively small changes.

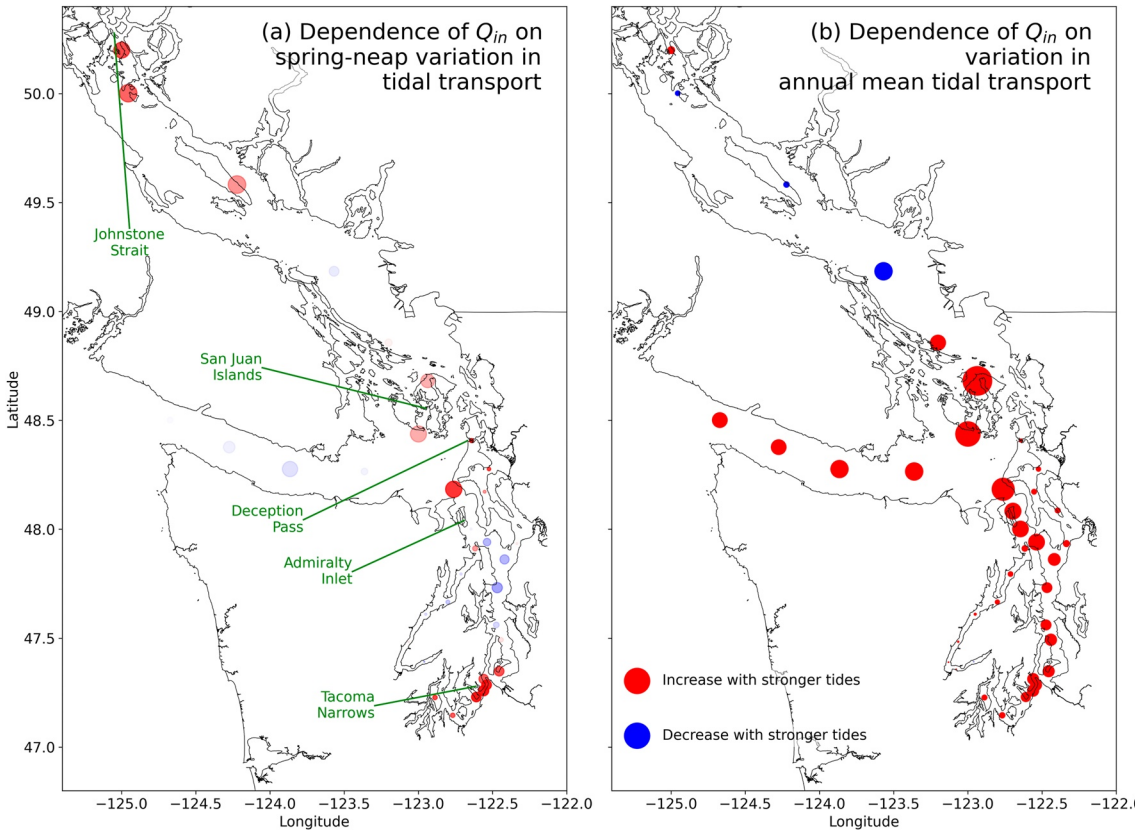

Figure 10. Maps of the dependence of exchange flow landward volume transport, Q_{in}, at all TEF sections due to variation in the strength of the tides, Q_{prism}. In (a) the variation is due to the spring-neap cycle as in Figure 5b. In (b) the variation is from the difference of annual means between the 110% and 75% tide manipulation experiments. The size of the circles is proportional to the amount of variation of transport. Red circles mean that transport increased with stronger tides, while blue circles mean that it decreased. The opacity of the circles in (a) is greater when the magnitude of the correlation coefficient of the linear fit used to calculate the variation is higher.

5. Spring neap variation of ΔS shows that it decreases with stronger tides, as would be expected with increased vertical mixing.
6. The annual mean system response to the tide manipulations shows that the mean salinity drops with stronger tides. The sign of this change is consistent with pure gravitational circulation (Figure 1b) and inconsistent with pure tidal pumping. However, the conflicting signs of the responses for Q_{in} and ΔS summarized above show that neither dynamical paradigm offers a complete description.

These results may help in understanding the dynamical functioning of estuaries with complex bathymetry and strong tides. Clearly tidal pumping cannot be neglected; neither is it the whole story. Similarly, the widely-accepted paradigm that the exchange flow and stratification increase at neap tides (Geyer & Cannon, 1982) appears to be locally valid at the part of Admiralty Inlet they studied (near our section **ai4**) but is not true at other places on that sill. We hope that the analysis methods and results presented here will provide tools to use and hypotheses to disprove for future research.

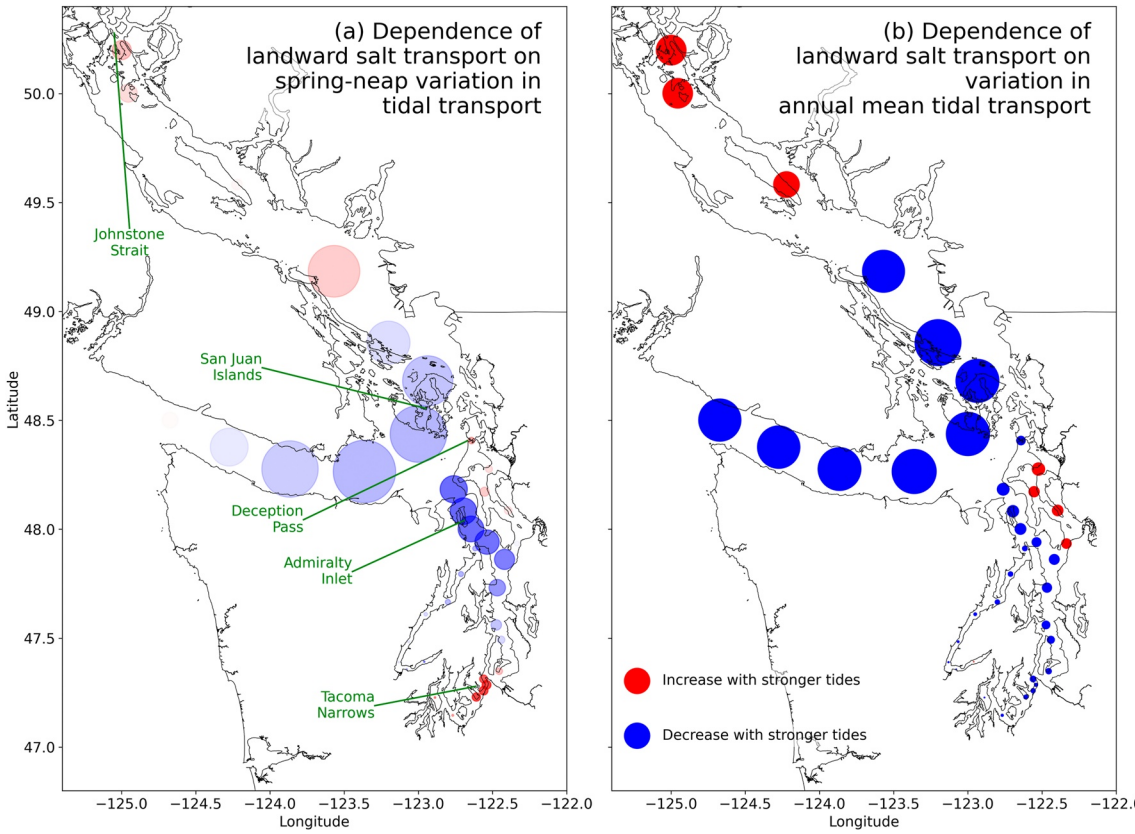

Figure 11. Maps of the dependence of landward salt transport, $Q_{in}\Delta S$, at all TEF sections due to variation in the strength of the tides, Q_{prism}. In (a) the variation is due to the spring-neap cycle as in Figure 5d. In (b) the variation is from the difference of annual means between the 110% and 75% tide manipulation experiments. The size of the circles is proportional to the amount of variation of salt transport. Red circles mean that salt transport increased with stronger tides, while blue circles mean that it decreased. The opacity of the circles in (a) is greater when the magnitude of the correlation coefficient of the linear fit used to calculate the variation is higher.

Data Availability Statement

All the model extractions and the code used to make all the figures is available at MacCready (2023) https://doi.org/10.5281/zenodo.10206345.

Acknowledgments
PM was supported by NSF Grant OCE-2122420. WRG was supported by NSF Grant OCE-2123002.

References

Aristizábal, M. F., & Chant, R. J. (2013). A numerical study of salt fluxes in Delaware Bay estuary. *Journal of Physical Oceanography*, *43*(8), 1572–1588. https://doi.org/10.1175/jpo-d-12-0124.1

Aristizábal, M. F., & Chant, R. J. (2015). An observational study of salt fluxes in Delaware Bay. *Journal of Geophysical Research: Oceans*, *120*(4), 2751–2768. https://doi.org/10.1002/2014jc010680

Banas, N. S., Hickey, B. M., MacCready, P., & Newton, J. A. (2004). Dynamics of Willapa Bay, Washington: A highly unsteady, partially mixed estuary. *Journal of Physical Oceanography*, *34*(11), 2413–2427. https://doi.org/10.1175/jpo2637.1

Becker, M. L., Luettich, R. A., & Seim, H. (2009). Effects of intratidal and tidal range variability on circulation and salinity structure in the Cape Fear River Estuary, North Carolina. *Journal of Geophysical Research*, *114*(C4), 1–20. https://doi.org/10.1029/2008jc004972

Bowen, M. M., & Geyer, W. R. (2003). Salt transport and the time-dependent salt balance of a partially stratified estuary. *Journal of Geophysical Research*, *108*(C5), 3158. https://doi.org/10.1029/2001JC001231

Bretschneider, D. E., Cannon, G. A., Holbrook, J. R., & Pashinski, D. J. (1985). Variability of subtidal current structure in a fjord estuary: Puget Sound, Washington. *Journal of Geophysical Research*, *90*(C6), 11949–11958. https://doi.org/10.1029/JC090iC06p11949

Broatch, E. M., & MacCready, P. (2022). Mixing in a salinity variance budget of the Salish Sea is controlled by river flow. *Journal of Physical Oceanography*, *52*(10), 2305–2323. https://doi.org/10.1175/jpo-d-21-0227.1

Burchard, H., Bolding, K., Feistel, R., Gräwe, U., Klingbeil, K., MacCready, P., et al. (2018). The Knudsen theorem and the total exchange flow analysis framework applied to the Baltic Sea. *Progress in Oceanography*, *165*, 268–286. https://doi.org/10.1016/j.pocean.2018.04.004

Cannon, G. A., Laird, N. P., & Keefer, T. L. (1979). Puget Sound circulation: Final report for FY77-78.

Chant, R. J., & Wilson, R. E. (2000). Internal hydraulics and mixing in a highly stratified estuary. *Journal of Geophysical Research*, *105*(C6), 14215–14222. https://doi.org/10.1029/2000JC900049

Chen, S.-N. (2017). Bathymetric influences on the estuarine equilibrium length and adjustment time. *Journal of Physical Oceanography*, *47*(7), 1719–1736. https://doi.org/10.1175/JPO-D-16-0075.1

Chen, S.-N., Geyer, W. R., Ralston, D. K., & Lerczak, J. A. (2012). Estuarine exchange flow quantified with isohaline coordinates: Contrasting long and short estuaries. *Journal of Physical Oceanography*, *42*(5), 748–763. https://doi.org/10.1175/jpo-d-11-086.1

Cloern, J. E., Foster, S. Q., & Kleckner, A. E. (2014). Phytoplankton primary production in the world's estuarine-coastal ecosystems. *Biogeosciences*, *11*(9), 2477–2501. https://doi.org/10.5194/bg-11-2477-2014

Cokelet, E. D., Stewart, R. J., & Ebbesmeyer, C. C. (1991). Concentrations and ages of conservative pollutants in Puget Sound. In *Paper presented at the Puget Sound research '91*.

Deppe, R. W., Thomson, J., Polagye, B., & Krembs, C. (2018). Predicting deep water intrusions to Puget sound, WA (USA), and the seasonal modulation of dissolved oxygen. *Estuaries and Coasts*, *41*(1), 114–127. https://doi.org/10.1007/s12237-017-0274-6

Dürr, H. H., Laruelle, G. G., van Kempen, C. M., Slomp, C. P., Meybeck, M., & Middelkoop, H. (2011). Worldwide typology of nearshore coastal systems: Defining the estuarine filter of river inputs to the oceans. *Estuaries and Coasts*, *34*(3), 441–458. https://doi.org/10.1007/s12237-011-9381-y

Ebbesmeyer, C. C., Word, J. Q., & Barnes, C. A. (1988). Puget Sound: A fjord system homogenized with water recycled over sills by tidal mixing. *Hydrodynamics of Estuaries: Volume II*, 17–29.

Farmer, D. M., & Freeland, H. J. (1983). The physical oceanography of Fjords. *Progress in Oceanography*, *12*(2), 147–219. https://doi.org/10.1016/0079-6611(83)90004-6

Fram, J. P., Martin, M. A., & Stacey, M. T. (2007). Dispersive fluxes between the coastal ocean and a semienclosed estuarine basin. *Journal of Physical Oceanography*, *37*(6), 1645–1660. https://doi.org/10.1175/jpo3078.1

Garcia, A. M. P., & Geyer, W. R. (2023). Tidal dispersion in short estuaries. *Journal of Geophysical Research: Oceans*, *128*(2), e2022JC018883. https://doi.org/10.1029/2022jc018883

Geyer, W. R., & Cannon, G. A. (1982). Sill processes related to deep water renewal in a fjord. *Journal of Geophysical Research*, *87*(C10), 7985–7996. https://doi.org/10.1029/JC087iC10p07985

Geyer, W. R., & MacCready, P. (2014). The estuarine circulation. *Annual Review of Fluid Mechanics*, *46*(1), 175–197. https://doi.org/10.1146/annurev-fluid-010313-141302

Geyer, W. R., Trowbridge, J. H., & Bowen, M. M. (2000). The dynamics of a partially mixed estuary. *Journal of Physical Oceanography*, *30*(8), 2035–2048. https://doi.org/10.1175/1520-0485(2000)030<2035:TDOAPM>2.0.CO;2

Giddings, S. N., Fong, D. A., & Monismith, S. G. (2011). Role of straining and advection in the intratidal evolution of stratification, vertical mixing, and longitudinal dispersion of a shallow, macrotidal, salt wedge estuary. *Journal of Geophysical Research*, *116*(C3), 1–20. https://doi.org/10.1029/2010JC006482

Giddings, S. N., & MacCready, P. (2017). Reverse estuarine circulation due to local and remote wind forcing, enhanced by the presence of along-coast estuaries. *Journal of Geophysical Research: Oceans*, *122*(12), 10184–10205. https://doi.org/10.1002/2016JC012479

Gregg, M. C., & Pratt, L. J. (2010). Flow and hydraulics near the sill of hood canal, a strongly sheared, continuously stratified fjord. *Journal of Physical Oceanography*, *40*(5), 1087–1105. https://doi.org/10.1175/2010JPO4312.1

Haas, L. W. (1977). The effect of the spring-neap tidal cycle on the vertical salinity structure of the James, York and Rappahannock Rivers, Virginia, U.S.A. *Estuarine and Coastal Marine Science*, *5*(4), 485–496. https://doi.org/10.1016/0302-3524(77)90096-2

Hansen, D. V., & Rattray, M., Jr. (1965). Gravitational circulation in straits and estuaries. *Journal of Marine Research*, *23*, 104–122.

Hughes, F. W. W., & Rattray, M. (1980). Salt flux and mixing in the Columbia River Estuary. *Estuarine and Coastal Marine Science*, *10*(5), 479–493. https://doi.org/10.1016/S0302-3524(80)80070-3

Jay, D. A., & Smith, J. D. (1990). Circulation, density distribution and neap-spring transitions in the Columbia River Estuary. *Progress in Oceanography*, *25*(1–4), 81–112. https://doi.org/10.1016/0079-6611(90)90004-L

LeBlond, P. H. (1983). The Strait of Georgia: Functional anatomy of a coastal sea. *Canadian Journal of Fisheries and Aquatic Sciences*, *40*(7), 1033–1063. https://doi.org/10.1139/f83-128

Lemagie, E. P., Giddings, S. N., MacCready, P., Seaton, C., & Wu, X. (2022). Measuring estuarine total exchange flow from discrete observations. *Journal of Geophysical Research: Oceans*, *127*(10), e2022JC018960. https://doi.org/10.1029/2022jc018960

Lerczak, J. A., Geyer, W. R., & Chant, R. J. (2006). Mechanisms driving the time-dependent salt flux in a partially stratified estuary. *Journal of Physical Oceanography*, *36*(12), 2296–2311. https://doi.org/10.1175/JPO2959.1

Lerczak, J. A., Geyer, W. R., & Ralston, D. K. (2009). The temporal response of the length of a partially stratified estuary to changes in river flow and tidal amplitude. *Journal of Physical Oceanography*, *39*(4), 915–933. https://doi.org/10.1175/2008JPO3933.1

Lorenz, M., Klingbeil, K., MacCready, P., & Burchard, H. (2019). Numerical issues of the total exchange flow (TEF) analysis framework for quantifying estuarine circulation. *Ocean Science Discussions*, *15*, 601–614. https://doi.org/10.5194/os-2018-147

MacCready, P. (2007). Estuarine adjustment. *Journal of Physical Oceanography*, *37*(8), 2133–2145. https://doi.org/10.1175/JPO3082.1

MacCready, P. (2011). Calculating estuarine exchange flow using isohaline coordinates. *Journal of Physical Oceanography*, *41*(6), 1116–1124. https://doi.org/10.1175/2011JPO4517.1

MacCready, P. (2023). Code and data for Salish exchange dynamics paper [Dataset]. Zenodo. https://doi.org/10.5281/zenodo.10206345

MacCready, P., & Banas, N. S. (2011). Residual circulation, mixing, and dispersion. In *Treatise on estuarine and coastal science* (Vol. 2, pp. 75–89). Elsevier.

MacCready, P., & Geyer, W. R. (2010). Advances in estuarine physics. *Annual Review of Marine Science*, *2*(1), 35–58. https://doi.org/10.1146/annurev-marine-120308-081015

MacCready, P., McCabe, R. M., Siedlecki, S. A., Lorenz, M., Giddings, S. N., Bos, J., et al. (2021). Estuarine circulation, mixing, and residence times in the Salish Sea. *Journal of Geophysical Research: Oceans*, *126*(2), e2020JC016738. https://doi.org/10.1029/2020jc016738

Mackas, D. L., & Harrison, P. J. (1997). Nitrogenous nutrient sources and sinks in the Juan de Fuca strait/strait of Georgia/Puget sound estuarine system: Assessing the potential for eutrophication. *Estuarine, Coastal and Shelf Science*, *44*, 1–21. https://doi.org/10.1006/ecss.1996.0110

Martin, W. D., & MacCready, P. (2011). Influence of large-scale tidal asymmetry on subtidal dynamics in the western Strait of Juan de Fuca. *Journal of Geophysical Research*, *116*(C2), 1–20. https://doi.org/10.1029/2010JC006363

Mofjeld, H. O., & Larsen, L. H. (1984). Tides and tidal currents of the inland waters of Western Washington. Retrieved from https://www.pmel.noaa.gov/pubs/PDF/mofj687/mofj687.pdf

Najjar, R. G., Herrmann, M., Alexander, R., Boyer, E. W., Burdige, D. J., Butman, D., et al. (2018). Carbon budget of tidal wetlands, estuaries, and shelf waters of eastern North America. *Global Biogeochemical Cycles*, *32*(3), 389–416. https://doi.org/10.1002/2017gb005790

Pawlowicz, R. (2002). Observations and linear analysis of sill-generated internal tides and estuarine flow in Haro Strait. *Journal of Geophysical Research*, *107*(C6), 3056. https://doi.org/10.1029/2000jc000504

Peters, H., & Bokhorst, R. (2001). Microstructure observations of turbulent mixing in a partially mixed estuary. Part II: Salt flux and stress. *Journal of Physical Oceanography*, *31*(4), 1105–1119. https://doi.org/10.1175/1520-0485(2001)031<1105:MOOTMI>2.0.CO;2

Ralston, D. K., Geyer, W. R., & Lerczak, J. A. (2008). Subtidal salinity and velocity in the Hudson River estuary: Observations and modeling. *Journal of Physical Oceanography*, *38*(4), 753–770. https://doi.org/10.1175/2007JPO3808.1

Seim, H. E., & Gregg, M. C. (1997). The importance of aspiration and channel curvature in producing strong vertical mixing over a sill. *Journal of Geophysical Research*, *102*(C2), 3451–3472. https://doi.org/10.1029/96jc03415

Stigebrandt, A. (1976). On the effect of barotropic current fluctuations on the two-layer transport capacity of a constriction. *Journal of Physical Oceanography*, *7*(1), 118–122. https://doi.org/10.1175/1520-0485(1977)007<0118:oteobc>2.0.co;2

Stommel, H., & Farmer, H. G. (1952). On the nature of estuarine circulation.

Thomson, R. E., & Huggett, W. S. (1980). M2 baroclinic tides in Johnstone Strait, British Columbia. *Journal of Physical Oceanography*, *10*, 1509–1539. https://doi.org/10.1175/1520-0485(1980)010<1509:MBTIJS>2.0.CO;2

Thomson, R. E., Mihály, S. F., & Kulikov, E. A. (2007). Estuarine versus transient flow regimes in Juan de Fuca Strait. *Journal of Geophysical Research*, *112*(C9), 1–25. https://doi.org/10.1029/2006JC003925

Wang, T., Geyer, W. R., Engel, P., Jiang, W., & Feng, S. (2015). Mechanisms of tidal oscillatory salt transport in a partially stratified estuary. *Journal of Physical Oceanography*, *45*(11), 2773–2789. https://doi.org/10.1175/JPO-D-15-0031.1

Whitney, M. M., Ullman, D. S., & Codiga, D. L. (2016). Subtidal exchange in eastern long island sound. *Journal of Physical Oceanography*, *46*(8), 2351–2371. https://doi.org/10.1175/JPO-D-15-0107.1

Xiong, J., Shen, J., & Qin, Q. (2021). Exchange flow and material transport along the salinity gradient of a long estuary. *Journal of Geophysical Research: Oceans*, *126*(5), e2021JC017185. https://doi.org/10.1029/2021jc017185